

# Hedgehog Controls Quiescence and Activation of Neural Stem Cells in the Adult Ventricular-Subventricular Zone

Mathieu Daynac,<sup>1</sup> Linda Tirou,<sup>1</sup> H el ene Faure,<sup>1</sup> Marc-Andr e Mouthon,<sup>2,3,4,5</sup> Laurent R. Gauthier,<sup>2,3,4,5</sup> Heidi Hahn,<sup>6</sup> Fran ois D. Boussin,<sup>2,3,4,5,7,\*</sup> and Martial Ruat<sup>1,7,\*</sup>

<sup>1</sup>CNRS, UMR-9197, Neurosciences Paris-Saclay Institute, 1 Avenue de la Terrasse, 91198 Gif-sur-Yvette, France

<sup>2</sup>CEA DSV IRCM SCSR, Laboratoire de Radiopathologie, 92265 Fontenay-aux-Roses, France

<sup>3</sup>INSERM

<sup>4</sup>Universit  Paris Sud

<sup>5</sup>Universit  Paris Diderot, Sorbonne Paris Cit 

UMR 967, 92265 Fontenay-aux-Roses, France

<sup>6</sup>Tumor Genetics Group, Institute of Human Genetics, University Medical Center, 37073 G ttingen, Germany

<sup>7</sup>Co-senior author

\*Correspondence: [boussin@cea.fr](mailto:boussin@cea.fr) (F.D.B.), [ruat@inaf.cnrs-gif.fr](mailto:ruat@inaf.cnrs-gif.fr) (M.R.)

<http://dx.doi.org/10.1016/j.stemcr.2016.08.016>

## SUMMARY

Identifying the mechanisms controlling quiescence and activation of neural stem cells (NSCs) is crucial for understanding brain repair. Here, we demonstrate that Hedgehog (Hh) signaling actively regulates different pools of quiescent and proliferative NSCs in the adult ventricular-subventricular zone (V-SVZ), one of the main brain neurogenic niches. Specific deletion of the Hh receptor Patched in NSCs during adulthood upregulated Hh signaling in quiescent NSCs, progressively leading to a large accumulation of these cells in the V-SVZ. The pool of non-neurogenic astrocytes was not modified, whereas the activated NSC pool increased after a short period, before progressively becoming exhausted. We also showed that Sonic Hedgehog regulates proliferation of activated NSCs *in vivo* and shortens both their G<sub>1</sub> and S-G<sub>2</sub>/M phases in culture. These data demonstrate that Hh orchestrates the balance between quiescent and activated NSCs, with important implications for understanding adult neurogenesis under normal homeostatic conditions or during injury.

## INTRODUCTION

Neural stem cells (NSCs) are found in the ventricular-subventricular zone (V-SVZ) of the lateral ventricles and in the subgranular zone (SGZ) of the hippocampus, the two main neurogenic niches in the adult mammalian brain (Fuentelba et al., 2012; Aimone et al., 2014). Adult NSCs in the V-SVZ mainly give rise to neurons that populate the olfactory bulbs (OBs) and oligodendrocytes in the corpus callosum. Pioneering work and more recent experiments have demonstrated that NSC divisions generate actively dividing transit amplifying cells (TACs) that form a pool of intermediate progenitors (Doetsch et al., 1999). These cells further differentiate into proliferating immature neuroblasts (Im. Nbs) that become migrating neuroblasts (Mig. Nbs), which integrate within the OBs to produce functional neurons critical for olfactory memory (Lepousez et al., 2013).

Quiescent and activated NSCs coexist in adult stem cell niches (Albizu et al., 2010). Quiescent NSCs (qNSCs) are slowly dividing cells that can survive antimetabolic drugs or irradiation; they can regenerate the V-SVZ, giving rise to new neurons (Doetsch et al., 1999; Daynac et al., 2013). In contrast, activated NSCs (aNSCs) are actively dividing and can be eliminated by antimetabolic drugs or irradiation (Pastrana et al., 2009; Daynac et al., 2013). Both qNSCs and aNSCs have astrocyte-like phenotypes and express glial

fibrillary acidic protein (GFAP) and the astrocyte-specific glutamate transporter, GLAST (Doetsch et al., 1999; Browd et al., 2006). However, the combination of markers allowing the isolation of the different prospective subpopulations of V-SVZ cells, including qNSCs, were identified only recently (Pastrana et al., 2009; Beckervordersandforth et al., 2010; Daynac et al., 2013; Codega et al., 2014; Mich et al., 2014). Furthermore, only limited knowledge exists on the gene-regulatory networks of quiescent and activated NSCs. Such information is of primary importance in understanding the mechanisms controlling V-SVZ maintenance and regeneration, and its role in diseases.

Among signaling pathways regulating the V-SVZ cell population, the Sonic Hedgehog (SHH) pathway (Briscoe and Th erond, 2013; Ferent et al., 2014) was shown to increase cell proliferation and modulate the migration of neuroblasts exiting this niche (Machold et al., 2003; Ahn and Joyner, 2005; Angot et al., 2008). The inactivation of Smoothed (SMO) receptor in cell types expressing the neuroepithelial marker Nestin suggests that this SHH signal transducer is required for maintaining the NSC population (Balordi and Fishell, 2007a). Activation of this pathway, through the conditional ablation of the main SHH receptor Patched (PTC) in GLAST-expressing cells, leads to a dramatic decrease in neurogenesis and a shift from an asymmetric to a symmetric mode of division in NSCs (Ferent et al., 2014). Type B1 NSCs are the primary GLI-expressing



population (Ihrie et al., 2011; Petrova et al., 2013), and SHH pathway activation is region dependent and more prevalent in the ventral SVZ associated with the production of specific neuronal progeny (Ihrie et al., 2011). NSCs in the V-SVZ can be also mobilized upon GLI1 inhibition to repair demyelinated lesions (Samanta et al., 2015). However, it is not well understood how quiescence is controlled in adult brain neurogenic niches, and the potential role of SHH signaling in its regulation has not been explored.

Here, we combine *in vitro* and *in vivo* analysis of both pharmacological and genetic activation of the SHH signaling pathway to explore its potential roles in different steps of neurogenesis. We identified prospective qNSCs, aNSCs, and their progeny from the adult mouse V-SVZ niche using immunofluorescence and fluorescence-activated cell sorting (FACS) techniques (Daynac et al., 2013; Pineda et al., 2013; Daynac et al., 2014) to characterize and quantify the effects of SHH signaling on the different types of V-SVZ cells. We unveil for the first time the effects of SHH signaling causing an increase in qNSC number and a faster cell cycle in aNSCs. Cell-cycle analysis by video microscopy revealed a shortening of both G<sub>1</sub> and S-G<sub>2</sub>/M phases of aNSCs in culture. Interestingly, genetic activation of SHH signaling led to a large and progressive accumulation of qNSCs, while after an early increase in the pool of aNSCs the number of aNSCs was drastically reduced and neurogenesis was progressively exhausted. Thus, we report an unsuspected new role for SHH signaling in the regulation of quiescence in the V-SVZ in the adult brain.

## RESULTS

### Accumulation of qNSCs and Decreased Neurogenesis Following Long-Term Activation of SHH Signaling *In Vivo*

To gain insight into the role of SHH signaling *in vivo* specifically in the V-SVZ, we examined the status of the various cell populations after conditional PTC deletion in *Glast*-expressing cells, which resulted in the activation of the SHH pathway in this neurogenic niche (Feret et al., 2014). For this, we used *Glast-CreERT2;Ptc<sup>WT/WT</sup>;R26R-YFP* offspring (called *YFP-PTC<sup>+/+</sup>*) and *Glast-CreERT2;Ptc<sup>fl/fl</sup>;R26R-YFP* (called *YFP-PTC<sup>-/-</sup>*), in which YFP expression is initiated by tamoxifen-mediated activation of the Cre recombinase that permanently marks all the progeny of the recombined cells. We previously observed a progressive decrease in the neurogenic process and a marked accumulation of NSCs in these mice (Feret et al., 2014). However, it is still unknown whether the accumulated NSCs were in their quiescent or activated state.

The progeny of NSCs was traced by following YFP expression in mice treated with tamoxifen and analyzed 6 months

later. We observed that the YFP expression level was dramatically affected in coronal brain sections of *YFP-PTC<sup>-/-</sup>* animals. This was especially obvious in the dorsal part of the V-SVZ enriched in neuroblasts (Figures 1A, 1A', 1B, 1B', 1E, and S1A–S1D) that were associated with the decrease of YFP-positive cells in the granular and glomerular olfactory bulb layers of *YFP-PTC<sup>-/-</sup>* mice observed previously (Feret et al., 2014). Neuroblasts labeled as DCX<sup>+</sup> cells (Brown et al., 2003), and TACs labeled as GFAP<sup>-</sup>MASH1<sup>+</sup> cells (Pastrana et al., 2009) (Figures S1E and S1F), were dramatically decreased in the YFP-recombined cells (Figures 1I–1K). These changes were specific to YFP-recombined cells since non-recombined cells showed no differences (Figures 1I–1K, gray bars).

NSCs were detected using combinations of GFAP/SOX2 (Moreno-Estelles et al., 2012; Ottone et al., 2014) and GFAP/S100β (Petrova et al., 2013) immunolabeling in cells lining the lateral ventricles (Figures 1C–1E', S1J, S1K, S1O, and S1P). We found an increase of NSCs (GFAP<sup>+</sup>SOX2<sup>+</sup> and GFAP<sup>+</sup>S100β<sup>-</sup> cells) in the YFP<sup>+</sup> but not in the YFP<sup>-</sup> fraction (Figures 1G and 1H, green versus gray bars), indicating that this increase is specific to YFP-recombined cells. These results suggest an accumulation of the NSC population after long-term activation of SHH signaling. To evaluate whether this accumulation was related to qNSCs, aNSCs, or both, we used an accurate YFP/GFAP/MASH1 immunolabeling strategy as GFAP<sup>+</sup>MASH1<sup>+</sup> cells represent aNSCs (Pastrana et al., 2009). Interestingly, the population of recombined aNSCs (YFP<sup>+</sup>GFAP<sup>+</sup>MASH1<sup>+</sup>) decreased 6 months after tamoxifen-induced PTC deletion, suggesting that the accumulation of total NSCs is due to qNSCs only (Figures 1I, S1E, and S1F).

Thus, these data suggest that persistent activation of the SHH signaling pathway in NSCs induces their accumulation in a quiescent state over the long term and a dramatic loss of aNSCs and their progeny *in vivo*.

### SHH Pathway Is Upregulated in qNSCs at Long Term after PTC Deletion

To confirm the results obtained *in situ* 6 months after PTC deletion we used a rapid and an efficient FACS method, which purifies and identifies the cells present in the mouse V-SVZ using a combination of NSC (LEX) and progenitor cell (EGFR and CD24) markers (Figure 2) (Capela and Temple, 2002; Doetsch et al., 2002; Pastrana et al., 2009; Daynac et al., 2013, 2015). This method enables to distinguish qNSCs (LEX<sup>bright</sup>EGFR<sup>-</sup>CD24<sup>-</sup>, hereafter called LEX<sup>bright</sup>) from aNSCs (LEX<sup>+</sup>EGFR<sup>+</sup>CD24<sup>-</sup>, hereafter called LEX<sup>+</sup>EGFR<sup>+</sup>), TACs (LEX<sup>-</sup>EGFR<sup>+</sup>CD24<sup>-</sup>, hereafter called EGFR<sup>+</sup>), Im. Nbs (LEX<sup>-</sup>EGFR<sup>+</sup>CD24<sup>+</sup>, hereafter called CD24<sup>+</sup>EGFR<sup>+</sup>), and Mig. Nbs (LEX<sup>-</sup>EGFR<sup>-</sup>CD24<sup>+</sup>, hereafter called CD24<sup>+</sup>) (Daynac et al., 2013). Since LEX-fluorescein isothiocyanate (FITC) antibody used to label NSCs has the

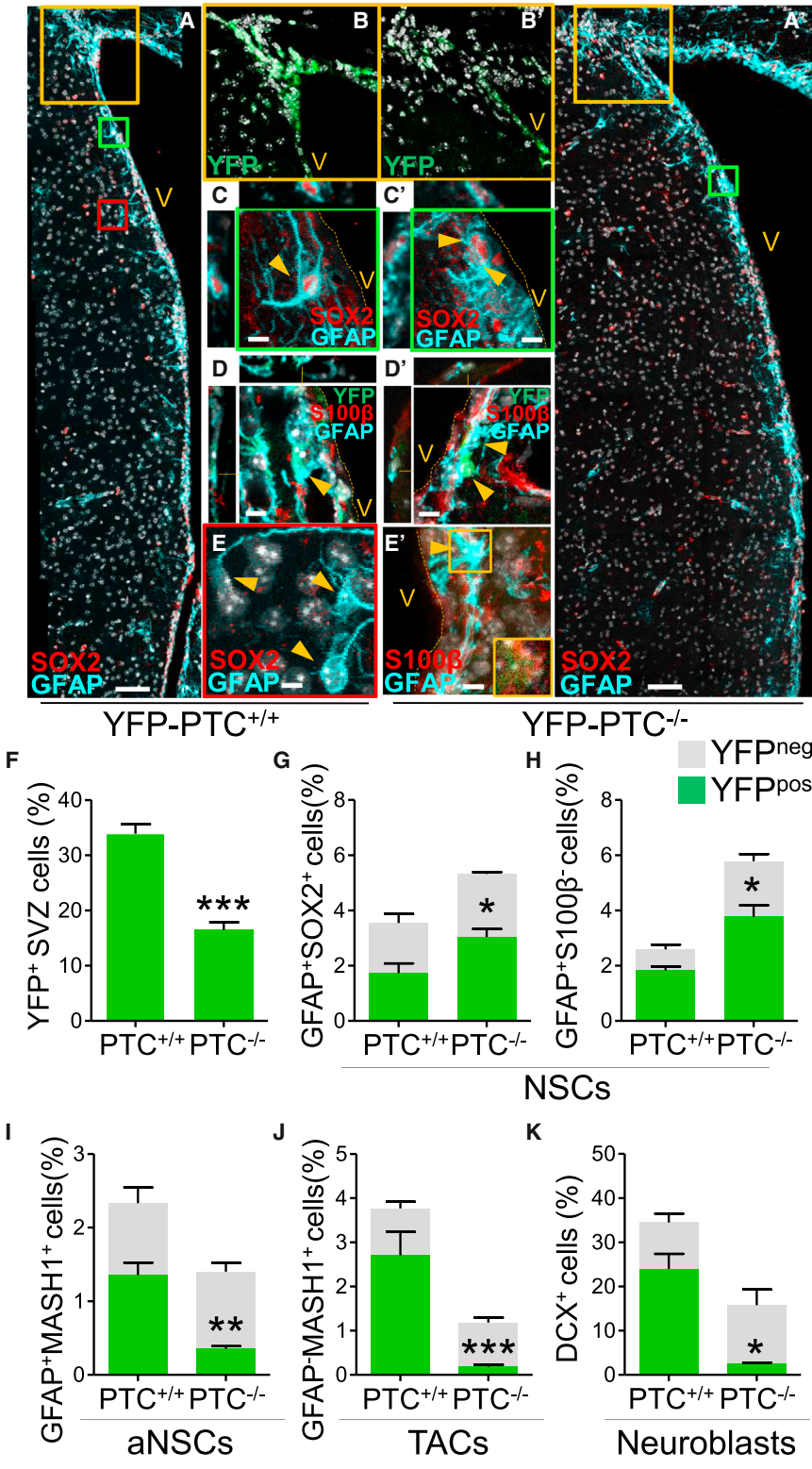


**Figure 1. Long-Term SHH Signaling Activation Induces a Decrease in Neurogenesis and an Accumulation of NSCs Specifically in YFP-Recombined Cells**

Data are derived from *YFP-PTC<sup>+/+</sup>* (A-E, F-K) versus *YFP-PTC<sup>-/-</sup>* (A'-E', F-K) mice 6 months after tamoxifen administration. (A, A') Immunostaining of coronal brain sections for NSC markers, GFAP and SOX2. (B, B') YFP expression in the dorsal V-SVZ (C, C') GFAP<sup>+</sup>SOX2<sup>+</sup> cells (NSCs; arrowheads) along the ventricle, (D, D') YFP<sup>+</sup>GFAP<sup>+</sup>S100β<sup>-</sup> cells (NSCs; arrowheads) along the ventricle, and (E, E') GFAP<sup>+</sup>SOX2<sup>-</sup> and YFP<sup>+</sup>GFAP<sup>+</sup>S100β<sup>+</sup> cells (mature astrocytes; arrowheads) (in E', S100β and YFP staining is shown in the bottom right corner). (F-K) Quantification of the V-SVZ populations using YFP/GFAP/SOX2, YFP/GFAP/S100β, YFP/GFAP/MASH1, or YFP/GFAP/DCX triple staining. Data are mean ± SEM obtained from brain analyses of four to five mice per phenotype in at least three different slices. \*p < 0.05, \*\*p < 0.01, \*\*\*p < 0.001 (for YFP cell analysis). Scale bars, 100 μm in (A, A') and 10 μm in (C-E'). See also Figure S1.

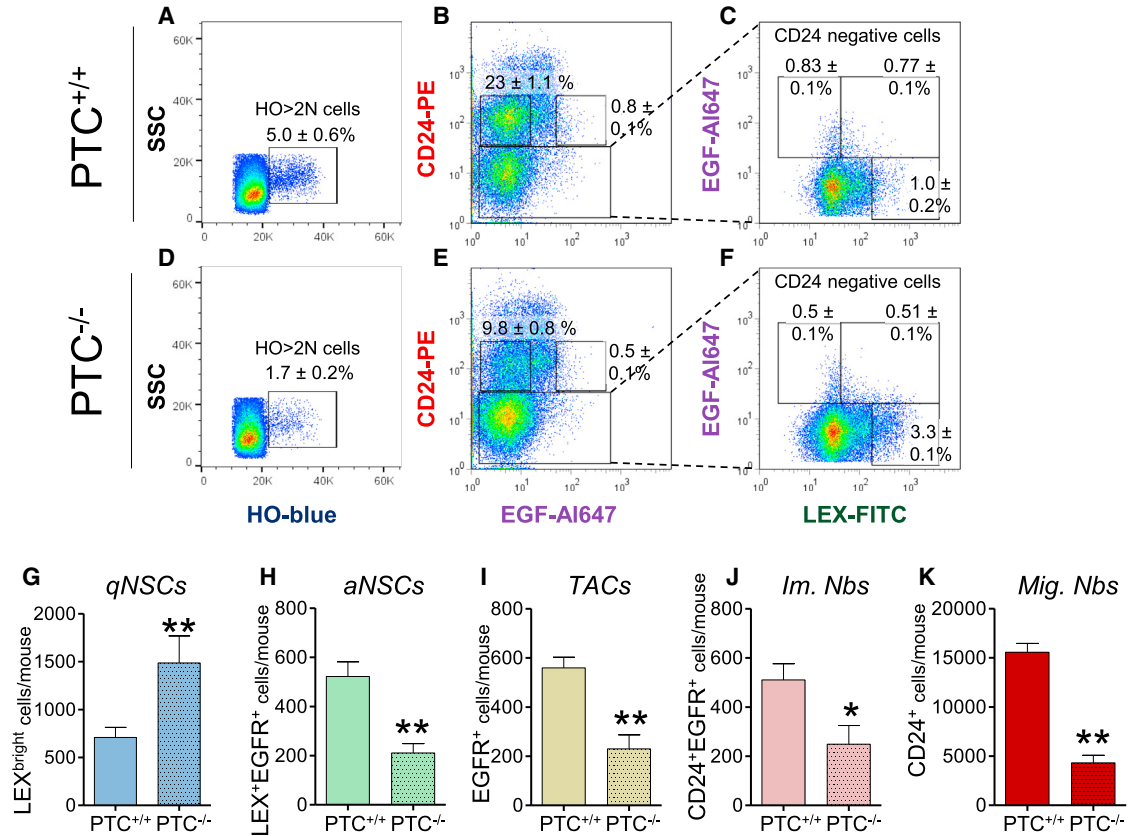


**Figure 2. Long-Term Activation of SHH Signaling Induces an Accumulation of qNSCs and a Decrease in Their Progeny**  
 Data are derived from  $PTC^{+/+}$  (A–C, G–K) versus  $PTC^{-/-}$  (D–K) mice 6 months after tamoxifen administration. (A, D) FACS plots representing V-SVZ proliferating cells (HO-blue is Hoechst 33342). (B, C, E, and F) Labeling of multiple cell populations from the V-SVZ along with the cell-sorting technique (see [Experimental Procedures](#)). (G–K) Quantification of the different V-SVZ populations sorted by FACS using TrueCount microbead-calibrated tubes in  $PTC^{+/+}$  (black boxes) and  $PTC^{-/-}$  (colored boxes) mice. Data represent mean ± SEM obtained from the independent analyses of cells isolated from ten mice (A–K) per phenotype, individually for each mouse. \* $p < 0.05$ , \*\* $p < 0.01$ . See also [Figures S2](#) and [S3](#).

same emission wavelength as YFP, we used non-YFP mice: *Glast-CreERT2;Ptc<sup>WT/WT</sup>* (called  $PTC^{+/+}$ ) and *Glast-CreERT2;Ptc<sup>fl/fl</sup>* (called  $PTC^{-/-}$ ). In  $PTC^{-/-}$  mice, 6 months after tamoxifen-induced PTC deletion, LEX<sup>+</sup>EGFR<sup>+</sup>, EGFR<sup>+</sup>, CD24<sup>+</sup>EGFR<sup>+</sup>, and CD24<sup>+</sup> populations were dramatically reduced by 59.5%, 58.9%, 51.2%, and 72.2%, respectively compared with  $PTC^{+/+}$  mice ([Figures 2H–2K](#)). Similarly, we observed a marked decrease in proliferating cells evaluated by Hoechst 33342 DNA content analysis (HO>2N cells [[Daynac et al., 2013](#)]; [Figures 2A, 2A', 2D, and 2D'](#)). In contrast, the cell fraction containing qNSCs (LEX<sup>bright</sup>) significantly increased by more than 2-fold ([Figure 2G](#)), which demonstrated that long-term genetic activation of SHH signaling leads to an accumulation of qNSCs. Interestingly, 6 months after PTC deletion the SHH pathway was specifically upregulated in qNSCs. This was concluded from the observation that *Gli1* levels used as a readout of SHH pathway activation were upregulated in qNSCs ([Briscoe and Therond, 2013](#);

[Ruat et al., 2014](#)), but not in aNSCs, TACs, and Im. Nbs ([Figure S2](#)).

Thus, these data demonstrate that long-term genetic deletion of PTC in GLAST-expressing cells results in a specific activation of SHH pathway in qNSCs, resulting in their accumulation in vivo while aNSCs and their progeny are dramatically decreased.

### Activation of SHH Signaling In Vivo Induces a Progressive Accumulation of qNSCs and Only a Transient Increase in aNSCs

To evaluate the short-term versus long-term effects of PTC deletion in vivo in YFP- $PTC^{+/+}$  versus YFP- $PTC^{-/-}$  mice, we used another FACS method that takes advantage of the GLAST NSC marker, along with EGFR and CD24 ([Figure 3A](#)) ([Mich et al., 2014](#)). Indeed, qNSCs were reported to have a GLAST<sup>bright</sup>EGFR<sup>-</sup>CD24<sup>-</sup> phenotype ([Mich et al., 2014](#)), and we found that GLAST<sup>bright</sup> correlates with LEX<sup>bright</sup>



NSC phenotype in CD24-negative cells (Figures S3A–S3C). Interestingly, short term after PTC deletion, we observed an accumulation of qNSCs (YFP<sup>+</sup>GLAST<sup>bright</sup>EGFR<sup>-</sup>CD24<sup>-</sup>), aNSCs (YFP<sup>+</sup>GLAST<sup>+</sup>EGFR<sup>+</sup>CD24<sup>-</sup>), and TACs (YFP<sup>+</sup>GLAST<sup>-</sup>EGFR<sup>+</sup>CD24<sup>-</sup>), but not their progeny (Figures 3B–3G). The pool of qNSCs increased continuously over longer time periods (6 months and then 10 months; Figures 3B–3G), while their progeny, including aNSCs, was progressively exhausted (Figures 3K–3M and S4). Ten months after PTC deletion, the number of qNSCs increased almost by 8-fold, and was  $\approx$  15-fold larger than the aNSC population (Figures 3H–3J). Strikingly, qNSCs did not seem to differentiate into astrocytes, as no accumulation of mature astrocyte population (GLAST<sup>dim</sup> expressing cells [Mich et al., 2014]) was observed (Figure S3D).

Thus, we prove that PTC deletion in GLAST-expressing cells triggers an initial accumulation of qNSCs, aNSCs, and their immediate progeny as a short-term effect. In contrast, the long-term effect involves accumulation of qNSCs over time while aNSCs and their progeny are progressively exhausted.

### SHH Pathway Activation Induces qNSC and aNSC Proliferation

Next, we evaluated the effects of SHH pathway activation on the proliferation of qNSCs and their progeny. We first performed intraventricular injections of SHH in young adult transgenic fluorescence ubiquitination cell-cycle indicator (FUCCI)-green mice that allow tracking the S-G<sub>2</sub>/M phases with green fluorescence (Sakaue-Sawano et al., 2008) (Figure 4). The number of proliferating qNSCs and aNSCs increased within a short time period (3 days) after intraventricular SHH injections, although the increase in qNSCs was not statistically significant ( $p = 0.06$ ) (Figures 4C and 4D). No short-term effect of SHH pathway activation was seen on TACs and neuroblast proliferation (Figures 4E and 4F). We evaluated long-term effects on cell proliferation with Hoechst 33342 DNA content analysis (Daynac et al., 2013) in YFP-PTC<sup>+/+</sup> and YFP-PTC<sup>-/-</sup> mice, 15 days and 10 months after tamoxifen injection (Figure 5). The pools of proliferating qNSCs and aNSCs expanded 15 days after PTC deletion (Figures 5A and 5B), contrary to their progeny (Figures 5C–5E). Long-term activation of the SHH pathway (10 months after PTC deletion) resulted in a complete abrogation of proliferating aNSCs, TACs, Im. Nbs, and Mig. Nbs (Figures 5G–5J). In contrast, some qNSCs continued proliferating, though to a lesser extent (Figure 5F).

### SHH Increases the Neurosphere-Forming Potential and Shortens the Cell Cycle of Adult aNSCs In Vitro

To understand the short-term effect of SHH specifically on the proliferation of aNSCs and not their progeny, we con-

ducted an in-depth study on the cell-cycle dynamics of aNSCs versus TACs and Im. Nbs in vitro. Following FACS with LEX/EGFR/CD24 marker combination in V-SVZ cells from the adult mouse, we previously showed that aNSCs, TACs, and Im. Nbs cells exhibit a capacity to generate neurospheres in vitro, contrary to qNSCs and Mig. Nbs (Daynac et al., 2013, 2015). Using this method, we observed that SHH (10 nM) treatment increased the potential of aNSCs to form colonies in vitro (number of primary neurospheres generated) by almost 2-fold, but did not increase the potential of TACs or Im. Nbs to form colonies (Figures 6A–6C).

Moreover, the amount of generated cells, evaluated as neurosphere size from the cell-sorted populations 5 days after plating (Daynac et al., 2014), significantly increased for aNSCs after SHH treatment, but not for TACs or Im. Nbs (Figures 6D–6F). These data suggest that SHH increased the number of cells generated by aNSCs, probably by acting on their cell cycle. We thus used time-lapse video microscopy to test whether activation of SHH signaling would have direct effects on cell-cycle progression of LEX<sup>+</sup>EGFR<sup>+</sup> and EGFR<sup>+</sup> cells isolated from young adult mice (2 months of age) (Costa et al., 2011; Daynac et al., 2014, 2015). As expected from the results above, the cell-cycle length of EGFR<sup>+</sup> cells was not altered by SHH (10 nM) treatment whereas that of LEX<sup>+</sup>EGFR<sup>+</sup> cells was significantly shortened, from  $12.2 \pm 1.9$  hr to  $8.9 \pm 2.1$  hr ( $p < 0.01$ ; Figure S5).

To confirm these results and explore the cell-cycle progression of aNSCs and TACs in detail, we sorted these cell populations from the V-SVZ of adult transgenic FUCCI mice (Sakaue-Sawano et al., 2008). Next, we measured the lengths of the G<sub>1</sub> phase (FUCCI-red fluorescence) and the S-G<sub>2</sub>/M phases (colorless), using time-lapse video microscopy, for cells that completed a full division and underwent at least another subsequent division to exclude any alteration due to cell-cycle exit (Daynac et al., 2014, 2015). As expected, the lengths of G<sub>1</sub> and S-G<sub>2</sub>/M phases were similar in non-treated and SHH-treated EGFR<sup>+</sup> cells (Figures 7A and 7C), leading to similar cell-cycle lengths (Figure 7D). In contrast, both G<sub>1</sub> and S-G<sub>2</sub>/M phases were shortened by almost 1 hr in LEX<sup>+</sup>EGFR<sup>+</sup> cells treated with SHH (1.1 hr and 0.8 hr, respectively; Figures 7A and 7B), leading to a shortening of the total cell cycle by 1.9 hr (Figure 7D) (Palma et al., 2005). Together, these results demonstrate that activation of the SHH pathway in vitro increases aNSC proliferation by shortening both G<sub>1</sub> and S-G<sub>2</sub>/M phases of their cell cycle. Finally, we investigated whether a pharmacological blockade of the Hh pathway could modify the cell-proliferation effect observed above (Figures S7A–S7K). Treatment with the Smo antagonist MRT-83 (1  $\mu$ M) (Roudaut et al., 2011; Hoch et al., 2015) reduced the number and size of neurospheres produced by aNSCs



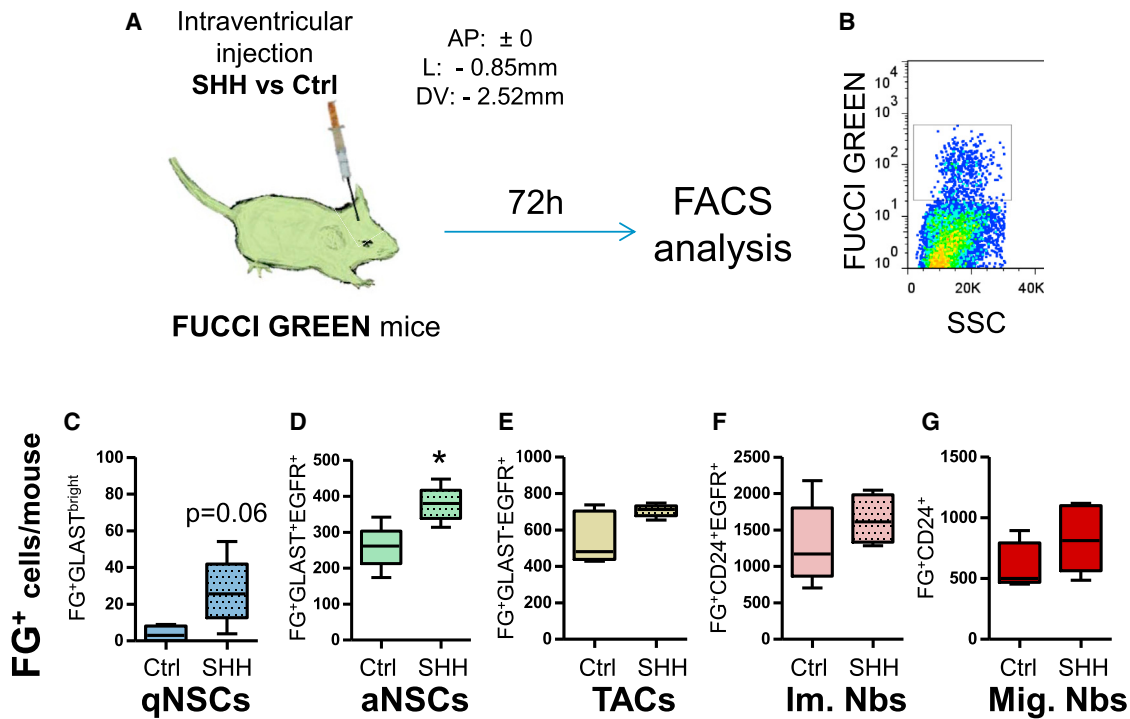


**Figure 4. Intraventricular Injection of SHH Increases NSC Proliferation In Vivo at Short Term**

(A) FUCCI-green mice (Sakaue-Sawano et al., 2008) that allow tracking the S-G<sub>2</sub>/M phases with green fluorescence received intraventricular injections of SHH (3 μg; AP: ±0 mm, L: -0.85 mm, DV: -2.52 mm) versus Ctrl (vehicle) and FUCCI-green-positive (FG<sup>+</sup>) cells were analyzed by FACS 72 hr after injection, using a FUCCI-green/GLAST-PE/EGF-647/CD24-PEcy7 quadruple staining.

(B–G) SHH injection provoked an increase in FG<sup>+</sup> proliferating qNSCs (p = 0.06) and aNSCs (D, E) while no difference was observed for their progeny (C–G).

Data represent mean ± SEM obtained from the independent analyses of cells isolated from five Ctrl versus five SHH mice, individually for each mouse. \*p < 0.05.

in vitro (Figures S7A and S7B), mirroring in vitro data with SHH (Figures 6A and 6D). The number of proliferating qNSCs and aNSCs from the V-SVZ populations was decreased on short-term (3 days) intraventricular MRT-83 injection in FUCCI-green mice, although not significantly for aNSCs (Figures S7G and S7H), probably due to the low basal expression of the pathway in aNSCs (Figure S2).

Together, these data show that activation of the SHH pathway in GLAST-expressing cells triggers an early phase marked by an increase in the proliferation of both qNSCs and aNSCs, leading to an early expansion of their pool. However, long-term activation of the SHH pathway in aNSCs led to progressive depletion of their pool and a collapse of neurogenesis (Figure S6). These findings show that the SHH pathway is essential for maintaining neuro-

genesis during adulthood by controlling the activation of qNSCs.

## DISCUSSION

Self-renewal of NSCs contributes to maintaining neurogenesis in the adult brain throughout life. Neurogenesis is actively involved in odor discrimination and cognitive performance that decrease upon aging (Lepousez et al., 2013; Aimone et al., 2014). In the V-SVZ, NSCs also generate oligodendrocytes (Menn et al., 2006). However, the precise molecular mechanisms controlling NSC pool size are not yet well understood. Using newly developed methods that identify the main cell populations of the V-SVZ and

(H–M) Quantification of the absolute number of qNSCs (blue) and aNSCs (green) populations sorted by FACS using TrueCount microbead-calibrated tubes. Data represent means ± SEM obtained from the independent analyses of cells isolated from five mice per phenotype for each time point, individually for each mouse.

\*p < 0.05, \*\*p < 0.01. See also Figure S4.

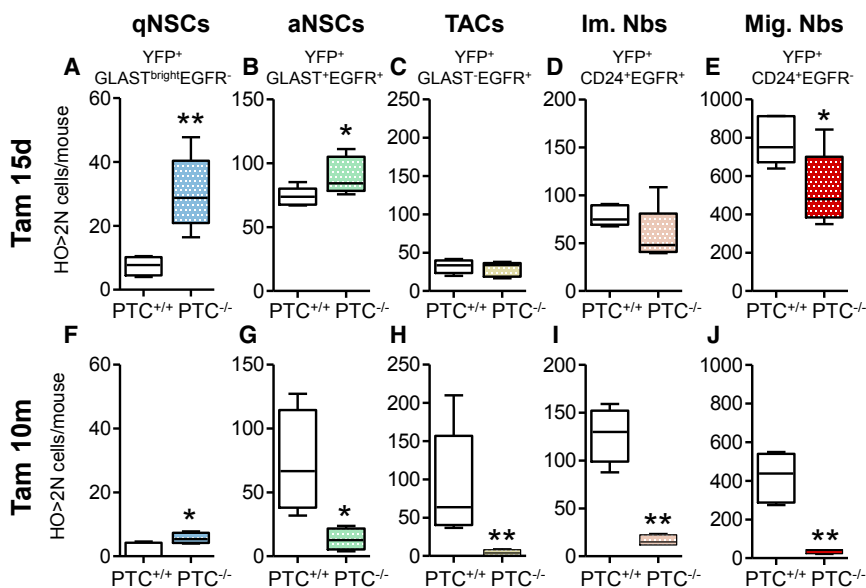


**Figure 5. SHH Pathway Activation Stimulates qNSC and aNSC Proliferation at Short Term, but Depletes the Pool of Proliferating aNSCs at Long Term**

Quantification of the number of S-G<sub>2</sub>/M proliferating cells (HO>2N) in the different V-SVZ populations sorted by FACS using TrueCount microbead-calibrated tubes from *YFP-PTC*<sup>+/+</sup> (white boxes) and *YFP-PTC*<sup>-/-</sup> (colored boxes) mice 15 days (15 d; A–E) and 10 months (10 m; F–J) after tamoxifen (Tam)-induced PTC deletion. Cell proliferation status is analyzed by DNA content analysis using Hoechst 33342 (Daynac et al., 2013). Data represent means ± SEM obtained from the independent analyses of cells isolated from five mice per phenotype for each time point, individually for each mouse. \*p < 0.05, \*\*p < 0.01.

a genetic mouse model of SHH activation in NSCs, our study identifies a crucial role of the SHH pathway in the balance between qNSCs and aNSCs in the adult brain, and demonstrates that SHH actively regulates cell quiescence in the V-SVZ.

The recent ability to purify quiescent NSCs from the adult brain and the development of markers enabling their identification *in vivo* have opened novel avenues for investigating the mechanisms responsible for maintaining these cells in quiescence (Beckervordersandforth et al., 2010; Codega et al., 2014; Daynac et al., 2014; Mich et al., 2014). Here we used a combination of two sets of validated markers, LEX, EGFR, CD24 (Daynac et al., 2013) and GLAST, EGFR, CD24 (Mich et al., 2014), to prospectively isolate by FACS qNSCs, aNSCs, and their progeny. Following this we analyzed the effects of pharmacological and genetic activation of SHH signaling in these cell populations. We validated the data obtained from the FACS-sorted cells by analyzing the distribution and localization of these cells from *YFP-PTC*<sup>+/+</sup> and *YFP-PTC*<sup>-/-</sup> mice, using an accurate immunolabeling strategy (GFAP/MASH1/DCX). This enabled us to selectively identify qNSCs, aNSCs, TACs, and neuroblasts.

Actively dividing B1 cells (aNSCs in our study) were shown to go through three rounds of divisions before differentiating into C cells (referred as TACs in our study) (Ponti et al., 2013). However, the mechanisms regulating their behavior both *in vitro* and *in vivo* are still not known. Our study takes advantage of the unequivocal identification of aNSCs and TACs to show that cultured aNSCs and TACs have similar cell-cycle lengths ( $T_c \approx 13$  hr), confirming the previous *in vivo* study (Ponti et al., 2013). In addition,

we also showed that aNSCs but not TACs proliferate following SHH treatment by reducing their  $T_c$  by almost 2 hr. A striking observation is that the duration of both G<sub>1</sub> and S-G<sub>2</sub>/M phases of aNSCs are affected, suggesting that both phases are implicated in the proliferative effects. This specificity at the NSC level is likely due to the degree of SHH pathway activation within the different cell types linked to increased *Gli1* transcription, as we observed *in vivo*, and might also directly be related to GLI3 repressor activity that is critical for maintaining V-SVZ NSC function in the adult (Petrova et al., 2013). We hypothesized that within qNSCs, the level of SHH pathway activation is low to control the balance between quiescence and activation; whereas an increase in SHH signaling deregulates this balance and leads to an expansion of this pool, as we observed *in vivo*. Our findings corroborate those reported for Hh signaling in the developing vertebrate retina, supporting an increase of transient amplifying progenitor proliferation by speeding up their cell cycles and reducing both their G<sub>1</sub> and G<sub>2</sub> phases (Locker et al., 2006).

We observed that genetic activation of SHH signaling induced a progressive increase in qNSC numbers and a marked reduction of the aNSC pool, leading to an almost complete exhaustion of neurogenesis in the long-term and early aging of V-SVZ niches compared with mice displaying basal SHH activation (Figure S5). Interestingly, we identified an initial transient period over the short term when aNSCs are actively proliferating, presumably by shortening both their G<sub>1</sub> and S-G<sub>2</sub>/M phases, as seen *in vitro*. *In vitro* results (Figures S7A and S7B) on isolated cells corroborates *in vivo* observations, suggesting that the positive effect of SHH pathway activation on aNSC

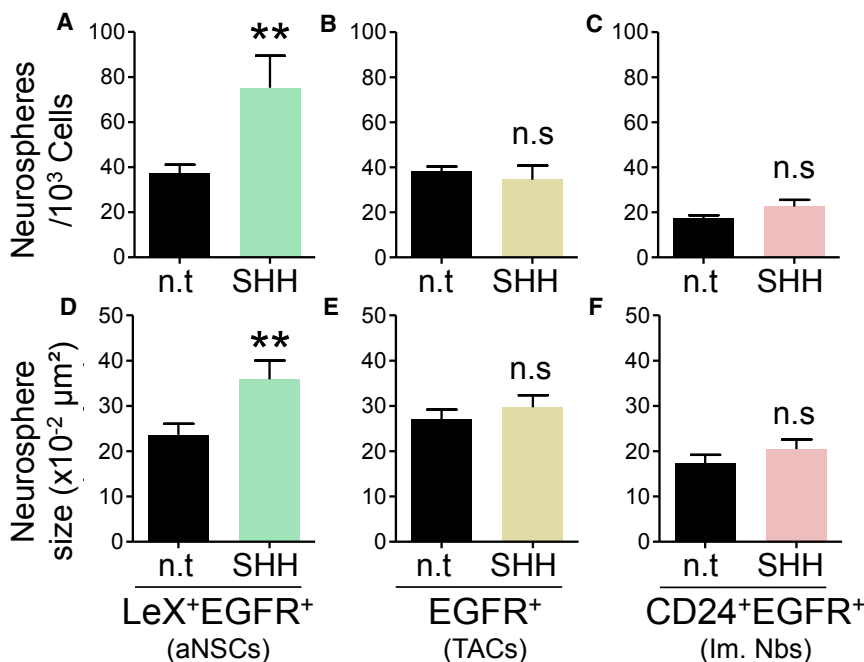


**Figure 6. SHH Treatment Increases the Neurosphere-Forming Potential of Activated NSCs**

LEX<sup>+</sup>EGFR<sup>+</sup> (A, D), EGFR<sup>+</sup> (B, E), and CD24<sup>+</sup>EGFR<sup>+</sup> (C, F) sorted cells from young adult mouse V-SVZ were plated and then treated with SHH (10 nM) or control buffer (n.t.). The neurosphere-forming potential (B–D) was determined as the number of neurospheres formed 7 days after plating, and the amount of cells generated (E, F) was evaluated as the area of the formed neurospheres 5 days after plating. Data represent mean ± SEM obtained from analyses of cells isolated from four to five independent groups of at least five mice. \*\*p < 0.01; n.s, not significant.

proliferation at short term occurs cell autonomously and is not triggered by microenvironmental changes. During this period, the number of TACs increases. This effect is not linked to a modification of their cell-cycle parameters, as shown in our study, but probably results from the differentiation of a high number of aNSCs that are produced. Migrating neuroblasts are also lowered. This could be explained by the abrogation of the chemoattractive activity that SHH exerts on V-SVZ-derived progenitors through PTC (Angot et al., 2008). Activation of the Hh pathway in NSCs through targeted injections of Ad:GFAPpCre virus in SmoM2-YFP;R26R mice was associated with an alteration of the type of progeny generated in the OB (Ihrie et al., 2011). There was no evidence of a collapse in neurogenesis but the study was not performed for a long period. The marked reduction of aNSCs over a longer term suggests that qNSC self-renewal is favored at the expense of aNSC production. NSCs appear to have a limited number of divisions (Balordi and Fishell, 2007b), which could explain that despite the expansion of aNSCs in the period shortly after SHH pathway activation, the low generation of new aNSCs in the long term leads to a significant decrease in their pool. A cell-autonomous defect in aNSCs associated with PTC deletion may also be responsible for this decrease. For example, aNSCs are also programmed to undergo a defined number of divisions prior to differentiation (Costa et al., 2011; Ponti et al., 2013), and the deletion of PTC in their membranes could alter the number of these divisions. Moreover, recent evidence suggests that aNSCs have limited self-renewal and are exhausted at long term (Calzo-

lari et al., 2015). The blockade of qNSCs in quiescence provoked by long-term PTC deletion seems to accelerate this phenomenon by reducing the availability of qNSCs needed to sustain neurogenesis over the long term.

Elevated SHH signaling in the dorsal V-SVZ regulates the production of oligodendrocyte progenitor cells in the corpus callosum while SHH signaling in the ventral V-SVZ controls the production of specific neuron subtypes destined for the OB (Tong et al., 2015). We previously observed that PTC deletion in NSCs decreases the ability of precursor cells to give rise to oligodendrocytes (Feret et al., 2014). It would be interesting to evaluate the effect of long-term PTC deletion on the production of specific neurons in the OB (Tong et al., 2015).

PTC inactivation in multipotent stem cells of human GFAP-Cre;PTC<sup>CIC</sup> mice during embryogenesis leads to medulloblastomas that develop when the cells have committed to the neuronal lineage (Yang et al., 2008). Our data demonstrate that PTC inactivation in NSCs increases the pool of qNSCs over the long term without the development of tumors, which demonstrates that the tumor-suppressor gene function of PTC (Goodrich et al., 1997) depends on the NSC context.

In sum, we uncovered that activation of the SHH pathway increases the pool of qNSCs over a long time period, thus demonstrating that active SHH signaling maintains V-SVZ cell quiescence. This is reminiscent of the recent role attributed to active Hh signaling engaged in an epithelial-mesenchymal regulatory loop to maintain quiescence under normal homeostasis in the adult lung

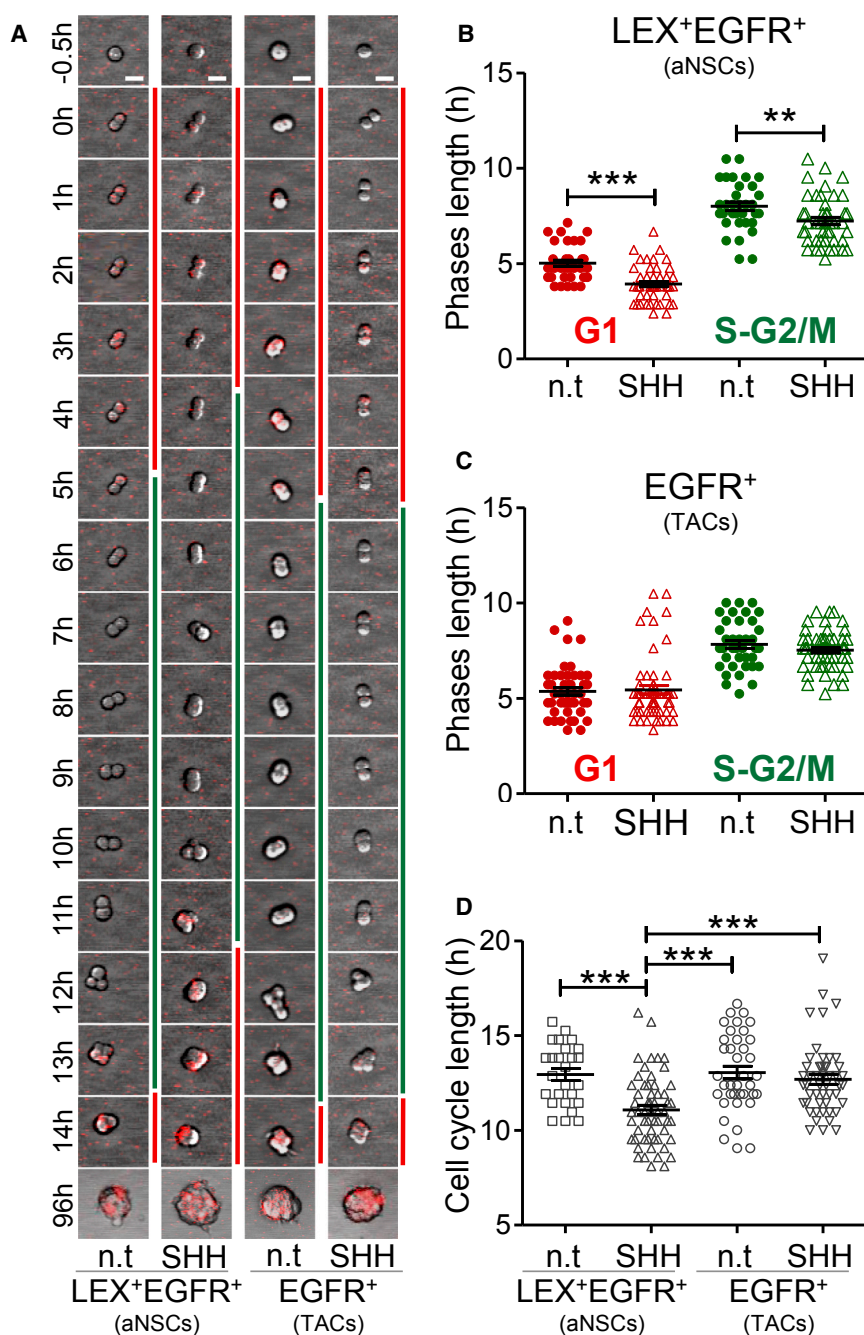


**Figure 7. SHH Shortens the Cell Cycle of Activated NSCs**

(A) Video microscopy with LEX<sup>+</sup>EGFR<sup>+</sup> (aNSCs) and EGFR<sup>+</sup> (TACs) V-SVZ cells sorted by FACS from Fucci-red mice (Sakaue-Sawano et al., 2008) allows tracking the G<sub>1</sub> phase with red fluorescence, whereas the S-G<sub>2</sub>/M phases are deduced when the red fluorescence switches off. Scale bars, 10 μm.

(B) The LEX<sup>+</sup>EGFR<sup>+</sup> cells had shorter G<sub>1</sub> and S-G<sub>2</sub>/M phases once treated with SHH (10 nM) compared with control treated conditions (n.t.).

(C) SHH treatment did not alter the G<sub>1</sub> and S-G<sub>2</sub>/M phases in EGFR<sup>+</sup> cells.

(D) The LEX<sup>+</sup>EGFR<sup>+</sup> cells had a shorter total cell-cycle length following SHH treatment, contrary to EGFR<sup>+</sup> cells. Data represent mean ± SEM obtained from cells isolated from two independent experiments with five mice.

\*\*p < 0.01, \*\*\*p < 0.001. See also Figures S5 and S6.

(Peng et al., 2015). Sustained SHH signaling in NSCs presumably occurs during physiological or pathological conditions, for instance, pharmacological activation of Smo using specific small-molecule modulators (Ruat et al., 2014), when SHH protein is induced (Ferent et al., 2013), or as a result of inactivating PTC or activating Smo mutations. Thus, it will be important to further identify the status of qNSCs and aNSCs in such conditions, as well as determine their effects on neurogenesis, tumor formation, and brain

repair. Of note, this accumulated pool of qNSCs has trouble replenishing the SVZ after antimitotic treatment (Ferent et al., 2014). Thus, it should be of great interest to address whether the increased pool of qNSCs observed upon SHH activation can be further manipulated in the older animal to restore impaired neurogenesis (Daynac et al., 2013) as observed with anti-transforming growth factor β treatment (Pineda et al., 2013; Daynac et al., 2014). Importantly, SHH signaling also regulates NSC mobilization toward



demyelinated lesions, and inhibition of GLI1 was shown to mobilize NSCs for remyelination (Samanta et al., 2015). Although the phenotype in qNSCs and aNSCs was not reported in this study, it indicates that multiple levels of SHH-GLI signaling regulate more than just proliferation and highlights the importance of determining the state of NSCs and their progeny. Altogether, our data highlight the complex role of the SHH pathway in NSC regulation and its importance for adult neurogenesis, and the need for further understanding of the mechanisms associated with brain tumor formation and brain repair.

## EXPERIMENTAL PROCEDURES

### Animals

*Glast-CreERT2;Ptc<sup>WT/WT</sup>;R26R-YFP* (called *YFP-PTC<sup>+/+</sup>*), *Glast-CreERT2;Ptc<sup>fl/fl</sup>;R26R-YFP* (called *YFP-PTC<sup>-/-</sup>*), *Glast-CreERT2;Ptc<sup>wt/wt</sup>* (called *PTC<sup>+/+</sup>*), and *Glast-CreERT2;Ptc<sup>fl/fl</sup>* (called *PTC<sup>-/-</sup>*) offspring were obtained as described by Ferent et al. (2014). For cell-cycle analysis, transgenic FUCCI chromatin labeling and DNA replication factor 1 (Cdt1)-red and (Geminin)-green mice were used (Sakaue-Sawano et al., 2008). Young adult (2–3 months old) C57Bl/6 mice were used for neurosphere and LEX versus GLAST FACS studies. Animal experiments were performed in compliance with the European Communities Council Directive (86/609/EEC) and were approved by our institution's ethics committee (11-003).

### Tamoxifen Administration, SHH Protein, and MRT-83 Injections

Tamoxifen (Sigma-Aldrich) was dissolved in corn oil (Sigma-Aldrich) at 10 mg/mL, and 1 mg was injected intraperitoneally twice a day for 5 consecutive days. Animals were killed 15 days, 6 months, or 10 months after the end of tamoxifen application. Male young adult FUCCI Green mice (five animals per group) were stereotactically injected into the right lateral ventricle of human SHHN (Biogen Idec) (5  $\mu$ L/3  $\mu$ g) or with the Smo antagonist MRT-83, which blocks Hh signaling in vitro and in vivo (2.5  $\mu$ L/200 ng), or the vehicle solutions as described previously (Loulier et al., 2006; Roudaut et al., 2011). MRT-83 was dissolved in 45% 2-hydroxypropyl- $\beta$ -cyclodextrin (Sigma) as described by Roudaut et al. (2011). A batch of SHHN was tested in a well-characterized assay of SHH function, the osteoblastic differentiation of C3H10T1/2 (Ruat et al., 2014). A subnanomolar concentration with SHHN (0.3 nM) led to a substantial increase in the response as previously reported (Loulier et al., 2006).

### Preparation of V-SVZ Cells and FACS

Lateral ventricle walls containing cells from the V-SVZ were microdissected and dissociated into single-cell suspensions as described by Daynac et al. (2013, 2015). For DNA content analysis, dissociated cells were incubated with Hoechst 33342 (Sigma), as described by Daynac et al. (2013). For mouse cell-surface marker analysis, we used GLAST phycoerythrin (PE) (mouse immunoglobulin G 2a [IgG2a]; 1:30, Miltenyi Biotec), CD24 PE/Cy7-conjugated (rat

IgG2b; 1:100, Biolegend), CD15/LEX fluorescein isothiocyanate (FITC)-conjugated (mouse IgM; 1:50, BD Biosciences), and Alexa 647-conjugated EGF ligand (1:200, Life Technologies). Cell proliferation status was analyzed by DNA content analysis using Hoechst 33342 (Daynac et al., 2013). The cells were transferred into tubes containing a calibrated number of fluorescent beads (Trucount tubes, BD Biosciences), analyzed on an LSRII (BD Biosciences) and sorted on an INFLUX (BD Biosciences), as reported by Daynac et al. (2013, 2015). Sorting gates were drawn according to FMO (fluorescence minus one) controls. The data were analyzed using FlowJo software (Tree Star).

### Immunofluorescence

Mice, under anesthesia, were perfused with 4% paraformaldehyde, and brain sections were cut on the cryostat (14  $\mu$ m) and processed for immunostaining, as reported by Daynac et al. (2013). The primary antibodies used were: mouse anti-GFAP (1:400, Mab3402, Millipore), rabbit polyclonal anti-GFAP (1:400, Sigma), goat anti-DCX (1:200, clone C-18 sc-8066, Santa Cruz Biotechnology), mouse anti-MASH1 (1:100, mAb556604, Becton Dickinson), mouse anti-SOX2 (1:100, mAb6F1.2, Millipore), and rabbit anti-S100B (1:200, mAbZ0311, Dako). Next, slices were incubated with the appropriate secondary antibody (Alexa Fluor series at 1:400, Invitrogen) for 2 hr at room temperature. Staining was replicated on at least three slices from three different parts of the SVZ in three different mice. z Stacks (from 5 to 20  $\mu$ m thick) containing 5–30 z sections were acquired on a laser-scanning confocal microscope (confocal Leica TCS SP8) with a 40 $\times$  oil objective (numerical aperture 0.75). Images were analyzed using LAS LF (Bitplane) and reconstructed in ImageJ 1.39t (NIH) and Photoshop CS3 (Adobe).

### Cultures of Sorted V-SVZ Cells

For neurosphere cultures, sorted cells were plated on poly-D-lysine-coated plates (Sigma) at a density of 1–3  $\times$  10<sup>3</sup> cells/well in 96-well tissue culture plates (TRP). The culture medium was composed of NeuroCult medium complemented with the proliferation supplement (STEMCELL Technologies), 2  $\mu$ g/mL heparin, 20 ng/mL EGF, and 10 ng/mL fibroblast growth factor 2. Seven days after plating, the neurospheres were counted and their area measured with ImageJ software. The cultures were incubated at 37°C in a humidified atmosphere containing 5% CO<sub>2</sub>. In vitro treatments with SHH (SHH C24II; R&D 1845-Sh) were done at 10 nM and with MRT-83 at 1  $\mu$ M.

### Live Cell Imaging

Freshly sorted cells were plated at a density of 1–3  $\times$  10<sup>3</sup> cells/well in poly-D-lysine-coated 96-well  $\mu$ -Plate culture plates (Ibidi). Live imaging culture conditions and settings were used as previously described (Daynac et al., 2014, 2015). Images and time-lapse video were analyzed with ImageJ and NIS-Elements AR.13.00 64-bit software.

### RT-PCR

Recombination efficiency was quantified by real-time PCR using specific primers for *wt PTC*, *PTC<sup>lox</sup>*, and *PTC<sup>del</sup>* alleles (Zibat et al., 2009). *Gli1*, *Gli2*, and *Gli3* primers were designed based on



Saqui-Salces et al. (2012): *mGli1 forward 5'-TTGGGATGAAGAAG CAGTTG-3', reverse 5'-GGAGACAGCATGGCTCACTA-3'; mGli2 forward 5'-ACCCAACACTCAGCAGCAGTAGC-3', reverse 5'-GCTCCGC TTATGAATGGTATGG-3'; mGli3 forward 5'-CAGCTCCACGACCA CTGAA-3', reverse 5'-CAGCTCCACGACCACTGAA-3'*. Despite a variation in YFP recombination among GLAST<sup>+</sup> cells dependent on mouse age, no variation was evidenced between *YFP-PTC<sup>+/+</sup>* and *YFP-PTC<sup>-/-</sup>* offspring for a given time point (data not shown). The deletion efficiency in *YFP-PTC<sup>-/-</sup>* mice was evaluated to 97.4% in *YFP<sup>+</sup>GLAST<sup>+</sup>* and 92.4% in *YFP<sup>+</sup>GLAST<sup>-</sup>* populations, respectively (data not shown).

### Cell Counting and Statistical Analyses

Non-parametric tests were conducted using StatView5 software (SAS Institute); the Kruskal-Wallis test associated with Dunn's multiple comparison test was used for multiple comparisons, and the Mann-Whitney test was used for two comparisons. The statistical significance was set at  $p < 0.05$ . The data are expressed as mean  $\pm$  SEM.

### SUPPLEMENTAL INFORMATION

Supplemental Information includes seven figures and can be found with this article online at <http://dx.doi.org/10.1016/j.stemcr.2016.08.016>.

### AUTHOR CONTRIBUTIONS

M.D.: conception and design, collection and assembly of data, data analysis and interpretation, and manuscript writing; L.T.: collection and assembly of data; H.F.: collection of data, data analysis and interpretation; M.M.: collection and assembly of data; L.R.G.: collection and assembly of data; H.H.: characterization of *YFP-PTC<sup>+/+</sup>* and *YFP-PTC<sup>-/-</sup>* mice; F.D.B.: conception and design, data analysis, interpretation, and manuscript writing; M.R.: conception, design, data analysis, interpretation, and manuscript writing.

### ACKNOWLEDGMENTS

We thank Prof. M. Götz (Helmholtz Zentrum, Munich) for *Glast-CreERT2* and S. Picaud (NeuroPSI, Gif/Yvette) for the mice used for initial breeding, Prof. T. Jessel (Columbia University) for R26R-YFP/+ mouse lines, and E. Desale and T. Durand (TAAM, CNRS UPS44, Orléans) for expert technical assistance. We are indebted to C. Joubert, V. Neuville, J. Tilliet, and the staff of the animal facilities, I. Baijer and N. Dechamps for cell sorting, and T. Kortulewski for imaging. L.T. is the recipient of a doctoral fellowship from the Ministère de la Recherche. This work was supported by grants from La Ligue contre le Cancer (Comité de l'Essonne), Fondation Association pour la Recherche contre le Cancer (ARC) and CNRS to M.R., and Électricité de France (EDF) to F.B.

Received: May 19, 2016

Revised: August 23, 2016

Accepted: August 23, 2016

Published: September 22, 2016

### REFERENCES

- Ahn, S., and Joyner, A.L. (2005). In vivo analysis of quiescent adult neural stem cells responding to Sonic hedgehog. *Nature* 437, 894–897.
- Aimone, J.B., Li, Y., Lee, S.W., Clemenson, G.D., Deng, W., and Gage, F.H. (2014). Regulation and function of adult neurogenesis: from genes to cognition. *Physiol. Rev.* 94, 991–1026.
- Albizu, L., Cottet, M., Kralikova, M., Stoev, S., Seyer, R., Brabet, I., Roux, T., Bazin, H., Bourrier, E., Lamarque, L., et al. (2010). Time-resolved FRET between GPCR ligands reveals oligomers in native tissues. *Nat. Chem. Biol.* 6, 587–594.
- Angot, E., Loulier, K., Nguyen-Ba-Charvet, K.T., Gadeau, A.P., Ruat, M., and Traiffort, E. (2008). Chemoattractive activity of sonic hedgehog in the adult subventricular zone modulates the number of neural precursors reaching the olfactory bulb. *Stem Cells* 26, 2311–2320.
- Balordi, F., and Fishell, G. (2007a). Hedgehog signaling in the subventricular zone is required for both the maintenance of stem cells and the migration of newborn neurons. *J. Neurosci.* 27, 5936–5947.
- Balordi, F., and Fishell, G. (2007b). Mosaic removal of hedgehog signaling in the adult SVZ reveals that the residual wild-type stem cells have a limited capacity for self-renewal. *J. Neurosci.* 27, 14248–14259.
- Beckervordersandforth, R., Tripathi, P., Ninkovic, J., Bayam, E., Lepier, A., Stempfhuber, B., Kirchhoff, F., Hirrlinger, J., Haslinger, A., Lie, D.C., et al. (2010). In vivo fate mapping and expression analysis reveals molecular hallmarks of prospectively isolated adult neural stem cells. *Cell Stem Cell* 7, 744–758.
- Briscoe, J., and Therond, P.P. (2013). The mechanisms of Hedgehog signalling and its roles in development and disease. *Nat. Rev. Mol. Cell Biol.* 14, 416–429.
- Browd, S.R., Kenney, A.M., Gottfried, O.N., Yoon, J.W., Walterhouse, D., Pedone, C.A., and Fults, D.W. (2006). N-myc can substitute for insulin-like growth factor signaling in a mouse model of sonic hedgehog-induced medulloblastoma. *Cancer Res.* 66, 2666–2672.
- Brown, J.P., Couillard-Despres, S., Cooper-Kuhn, C.M., Winkler, J., Aigner, L., and Kuhn, H.G. (2003). Transient expression of double-cortin during adult neurogenesis. *J. Comp. Neurol.* 467, 1–10.
- Calzolari, F., Michel, J., Baumgart, E.V., Theis, F., Gotz, M., and Ninkovic, J. (2015). Fast clonal expansion and limited neural stem cell self-renewal in the adult subependymal zone. *Nat. Neurosci.* 18, 490–492.
- Capela, A., and Temple, S. (2002). LEX/ssea-1 is expressed by adult mouse CNS stem cells, identifying them as nonependymal. *Neuron* 35, 865–875.
- Codega, P., Silva-Vargas, V., Paul, A., Maldonado-Soto, A.R., Deleo, A.M., Pastrana, E., and Doetsch, F. (2014). Prospective identification and purification of quiescent adult neural stem cells from their in vivo niche. *Neuron* 82, 545–559.
- Costa, M.R., Ortega, F., Brill, M.S., Beckervordersandforth, R., Petrone, C., Schroeder, T., Gotz, M., and Berninger, B. (2011).



Continuous live imaging of adult neural stem cell division and lineage progression in vitro. *Development* 138, 1057–1068.

Daynac, M., Chicheportiche, A., Pineda, J.R., Gauthier, L.R., Bousin, F.D., and Mouthon, M.A. (2013). Quiescent neural stem cells exit dormancy upon alteration of GABAAR signaling following radiation damage. *Stem Cell Res.* 11, 516–528.

Daynac, M., Pineda, J.R., Chicheportiche, A., Gauthier, L.R., Morizur, L., Boussin, F.D., and Mouthon, M.A. (2014). TGFbeta lengthens the G1 phase of stem cells in aged mouse brain. *Stem Cells* 32, 3257–3265.

Daynac, M., Morizur, L., Kortulewski, T., Gauthier, L.R., Ruat, M., Mouthon, M.A., and Boussin, F.D. (2015). Cell sorting of neural stem and progenitor cells from the adult mouse subventricular zone and live-imaging of their cell cycle dynamics. *J. Vis. Exp.* <http://dx.doi.org/10.3791/53247>

Doetsch, F., Caille, I., Lim, D.A., Garcia-Verdugo, J.M., and Alvarez-Buylla, A. (1999). Subventricular zone astrocytes are neural stem cells in the adult mammalian brain. *Cell* 97, 703–716.

Doetsch, F., Petreanu, L., Caille, I., Garcia-Verdugo, J.M., and Alvarez-Buylla, A. (2002). EGF converts transit-amplifying neurogenic precursors in the adult brain into multipotent stem cells. *Neuron* 36, 1021–1034.

Ferent, J., Zimmer, C., Durbec, P., Ruat, M., and Traiffort, E. (2013). Sonic Hedgehog signaling is a positive oligodendrocyte regulator during demyelination. *J. Neurosci.* 33, 1759–1772.

Ferent, J., Cochard, L., Faure, H., Taddei, M., Hahn, H., Ruat, M., and Traiffort, E. (2014). Genetic activation of Hedgehog signaling unbalances the rate of neural stem cell renewal by increasing symmetric divisions. *Stem Cell Rep.* 3, 312–323.

Fuentealba, L.C., Obernier, K., and Alvarez-Buylla, A. (2012). Adult neural stem cells bridge their niche. *Cell Stem Cell* 10, 698–708.

Goodrich, L.V., Milenkovic, L., Higgins, K.M., and Scott, M.P. (1997). Altered neural cell fates and medulloblastoma in mouse patched mutants. *Science* 277, 1109–1113.

Hoch, L., Faure, H., Roudaut, H., Schoenfelder, A., Mann, A., Girard, N., Bihannic, L., Ayrault, O., Petricci, E., Taddei, M., et al. (2015). MRT-92 inhibits Hedgehog signaling by blocking overlapping binding sites in the transmembrane domain of the Smoothed receptor. *FASEB J.* 29, 1817–1829.

Ihrle, R.A., Shah, J.K., Harwell, C.C., Levine, J.H., Guinto, C.D., Lezameta, M., Kriegstein, A.R., and Alvarez-Buylla, A. (2011). Persistent sonic hedgehog signaling in adult brain determines neural stem cell positional identity. *Neuron* 71, 250–262.

Lepousez, G., Valley, M.T., and Lledo, P.M. (2013). The impact of adult neurogenesis on olfactory bulb circuits and computations. *Annu. Rev. Physiol.* 75, 339–363.

Locker, M., Agathocleous, M., Amato, M.A., Parain, K., Harris, W.A., and Perron, M. (2006). Hedgehog signaling and the retina: insights into the mechanisms controlling the proliferative properties of neural precursors. *Genes Dev.* 20, 3036–3048.

Loulier, K., Ruat, M., and Traiffort, E. (2006). Increase of proliferating oligodendroglial progenitors in the adult mouse brain upon Sonic hedgehog delivery in the lateral ventricle. *J. Neurochem.* 98, 530–542.

Machold, R., Hayashi, S., Rutlin, M., Muzumdar, M.D., Nery, S., Corbin, J.G., Gritti-Linde, A., Dellovade, T., Porter, J.A., Rubin, L.L., et al. (2003). Sonic hedgehog is required for progenitor cell maintenance in telencephalic stem cell niches. *Neuron* 39, 937–950.

Menn, B., Garcia-Verdugo, J.M., Yaschine, C., Gonzalez-Perez, O., Rowitch, D., and Alvarez-Buylla, A. (2006). Origin of oligodendrocytes in the subventricular zone of the adult brain. *J. Neurosci.* 26, 7907–7918.

Mich, J.K., Signer, R.A., Nakada, D., Pineda, A., Burgess, R.J., Vue, T.Y., Johnson, J.E., and Morrison, S.J. (2014). Prospective identification of functionally distinct stem cells and neurosphere-initiating cells in adult mouse forebrain. *Elife* 3, e02669.

Moreno-Estelles, M., Gonzalez-Gomez, P., Hortiguera, R., Diaz-Moreno, M., San Emeterio, J., Carvalho, A.L., Farinas, I., and Mira, H. (2012). Symmetric expansion of neural stem cells from the adult olfactory bulb is driven by astrocytes via WNT7A. *Stem Cells* 30, 2796–2809.

Ottone, C., Krusche, B., Whitby, A., Clements, M., Quadrato, G., Pitulescu, M.E., Adams, R.H., and Parrinello, S. (2014). Direct cell-cell contact with the vascular niche maintains quiescent neural stem cells. *Nat. Cell Biol.* 16, 1045–1056.

Palma, V., Lim, D.A., Dahmane, N., Sanchez, P., Brionne, T.C., Herzberg, C.D., Gitton, Y., Carleton, A., Alvarez-Buylla, A., and Ruiz i Altaba, A. (2005). Sonic hedgehog controls stem cell behavior in the postnatal and adult brain. *Development* 132, 335–344.

Pastrana, E., Cheng, L.C., and Doetsch, F. (2009). Simultaneous prospective purification of adult subventricular zone neural stem cells and their progeny. *Proc. Natl. Acad. Sci. USA* 106, 6387–6392.

Peng, T., Frank, D.B., Kadzik, R.S., Morley, M.P., Rathi, K.S., Wang, T., Zhou, S., Cheng, L., Lu, M.M., and Morrissey, E.E. (2015). Hedgehog actively maintains adult lung quiescence and regulates repair and regeneration. *Nature* 526, 578–582.

Petrova, R., Garcia, A.D., and Joyner, A.L. (2013). Titration of GLI3 repressor activity by sonic hedgehog signaling is critical for maintaining multiple adult neural stem cell and astrocyte functions. *J. Neurosci.* 33, 17490–17505.

Pineda, J.R., Daynac, M., Chicheportiche, A., Cebrian-Silla, A., Sii Felice, K., Garcia-Verdugo, J.M., Boussin, F.D., and Mouthon, M.A. (2013). Vascular-derived TGF-beta increases in the stem cell niche and perturbs neurogenesis during aging and following irradiation in the adult mouse brain. *EMBO Mol. Med.* 5, 548–562.

Ponti, G., Obernier, K., Guinto, C., Jose, L., Bonfanti, L., and Alvarez-Buylla, A. (2013). Cell cycle and lineage progression of neural progenitors in the ventricular-subventricular zones of adult mice. *Proc. Natl. Acad. Sci. USA* 110, E1045–E1054.

Roudaut, H., Traiffort, E., Gorjankina, T., Vincent, L., Faure, H., Schoenfelder, A., Mann, A., Manetti, F., Solinas, A., Taddei, M., and Ruat, M. (2011). Identification and mechanism of action of the acylguanidine MRT-83, a novel potent smoothed antagonist. *Mol. Pharmacol.* 79, 453–460.

Ruat, M., Hoch, L., Faure, H., and Rognan, D. (2014). Targeting of Smoothed for therapeutic gain. *Trends Pharmacol. Sci.* 35, 237–246.



- Sakaue-Sawano, A., Kurokawa, H., Morimura, T., Hanyu, A., Hama, H., Osawa, H., Kashiwagi, S., Fukami, K., Miyata, T., Miyoshi, H., et al. (2008). Visualizing spatiotemporal dynamics of multicellular cell-cycle progression. *Cell* *132*, 487–498.
- Samanta, J., Grund, E.M., Silva, H.M., Lafaille, J.J., Fishell, G., and Salzer, J.L. (2015). Inhibition of Gli1 mobilizes endogenous neural stem cells for remyelination. *Nature* *526*, 448–452.
- Saqui-Salces, M., Coves-Datson, E., Veniaminova, N.A., Waghray, M., Syu, L.J., Dlugosz, A.A., and Merchant, J.L. (2012). Inflammation and Gli2 suppress gastrin gene expression in a murine model of antral hyperplasia. *PLoS One* *7*, e48039.
- Tong, C.K., Fuentealba, L.C., Shah, J.K., Lindquist, R.A., Ihrle, R.A., Guinto, C.D., Rodas-Rodriguez, J.L., and Alvarez-Buylla, A. (2015). A dorsal SHH-dependent domain in the V-SVZ produces large numbers of oligodendroglial lineage cells in the postnatal brain. *Stem Cell Rep.* *5*, 461–470.
- Yang, Z.J., Ellis, T., Markant, S.L., Read, T.A., Kessler, J.D., Bourbonnas, M., Schuller, U., Machold, R., Fishell, G., Rowitch, D.H., et al. (2008). Medulloblastoma can be initiated by deletion of Patched in lineage-restricted progenitors or stem cells. *Cancer Cell* *14*, 135–145.
- Zibat, A., Uhmman, A., Nitzki, F., Wijgerde, M., Frommhold, A., Heller, T., Armstrong, V., Wojnowski, L., Quintanilla-Martinez, L., Reifenberger, J., et al. (2009). Time-point and dosage of gene inactivation determine the tumor spectrum in conditional PTCh knockouts. *Carcinogenesis* *30*, 918–926.